Prospect of Thiazole-based γ-Peptide Foldamers in Enamine Catalysis: Exploration of the Nitro-Michael Addition

Julie Aguesseau-Kondrotas, Matthieu Simon, Baptiste Legrand, Jean-Louis Bantignies, Young Kee Kang, Dan Dumitrescu, Arie Van der lee, Jean-Marc Campagne, Renata Marcia de Figueiredo, Ludovic Maillard

HAL Id: hal-02167326

https://hal.umontpellier.fr/hal-02167326v1

Submitted on 2 Dec 2024

CHEMISTRY
A European Journal

Accepted Article

Title: Prospect of thiazole-based γ-peptide foldamers in enamine catalysis – exploration of the Nitro-Michael addition

Authors: Julie Aguesseau-Kondrotas, Matthieu Simon, Baptiste Legrand, Jean-Louis Bantigniès, Young Kee Kang, Dan Dumitrescu, Arie Van der Lee, Jean-Marc Campagne, Renata Marcia de Figueiredo, and Ludovic Thierry Maillard

WILEY-VCH

Prospect of thiazole-based γ-peptide foldamers in enamine catalysis – exploration of the Nitro-Michael addition

Julie Aguesseau-Kondrotas,[a] Matthieu Simon,[a] Baptiste Legrand,[a] Jean-Louis Bantigniès,[b] Young Kee Kang,[c] Dan Dumitrescu,[d] Arie Van der Lee,[e] Jean-Marc Campagne,[f] Renata Marcia de Figueiredo*[f] and Ludovic T. Maillard*[a]

Abstract: As a three-dimensional folding is prerequisite to biopolymer activities, complex functions may also be achieved through foldamer science. Because of the diversity of sizes, shapes and folding available with synthetic monomers, foldamer frameworks enable a numerous opportunities for designing new generations of catalysts. We herein demonstrate that heterocyclic γ–peptide scaffolds represent a versatile platform for enamine catalysis. One central feature was to determine how the catalytic activity and the transfer of chiral information might be under the control of the conformational behaviours of the oligomer.

Introduction

In protein, information encoded in the amino acid side chains directs the polypeptide backbone to fold into secondary, tertiary and ultimately quaternary structures enabling protein function. Enzymatic catalysis, for example depends on a well-defined three-dimensional fold to place side-chain functional groups in precise locations in an enzyme active site.[1-3] Efforts to understand the relationship among biopolymer sequence, structure and function have relied on simple structural motifs that recapitulate significant aspects of the behaviour of proteins. In this context, synthetic peptides decorated with catalytic artificial amino acid groups or transition metal sites have been demonstrated to be effective enantioselective catalysts due to the proximity of the catalytic sites to the asymmetric environment created by their backbone.[4-7] However, while some relevant successes in catalytic peptides, the development of short sequences that fold into defined secondary structures including helices, sheets and turns in organic or aqueous solution remains a challenge thus restricting their ability to recreate all the desirable characteristics of an enzyme catalyst. Because of the diversity of sizes, shapes and folding available with synthetic monomers, foldamer science now offers new attractive features to address this issue.[8-15] As in biopolymers, foldamers offer the possibility to create highly controlled molecular compartments that may settle the recognition and reactivity difficulties.[16]

Over the last years, our group explored a class of constrained heterocyclic γ-amino acids built around a thiazole ring, named ATCs. ATC oligomers showed high propensity to adopt a helical structure in the solid state and both organic solvents and water.[17, 18] Because of the highly azodi-carboxylateazodi-carboxylaterobust synthetic pathway that guarantees the access to a wide diversity of enantipure ATCs,[19] these foldamers could be readily functionalized. Importantly, the structure of the γ-peptide backbone showed low dependency on the nature of the side chains and the facial anisotropy of the platform ensures a perfect control of the spatial orientation of the appended functionalities.[20] Based on these properties, we herein considered ATC oligomers as a template for enamine organocatalysis. A key aspect of the program was to emphasize the relationship existing between the size and the substitution pattern of the foldamer and its catalytic properties.

Results and Discussion

Enamine catalysis[21-24] using proline or related catalysts has extensively been applied to both intermolecular and intramolecular nucleophilic addition reactions with a variety of electrophiles including imine in Mannich reaction [25-28], nitrosobenzene,[29-32] azodicarboxylates[33-35] and Michael acceptors. Considering both activity and selectivity, Wennemers tripeptide H-D-Pro-Pro-Glu-NH₂ (dPPE-NH₂) is probably the most efficient catalyst for diastereo- and enantioselective Michael addition of aldehydes to β-substituted nitro-olefins.[36-39] dPPE-NH₂ adopts a compact β-turn conformation[40] and its activity is drastically related to the presence of a suitably positioned carboxylic acid group in close proximity to the N-terminal secondary amine. The acidic group is assumed to orientate the reactivity and stereoselectivity of the reaction probably by coordinating the nitronate intermediate.[41] Furthermore it improves the reaction rate, by promoting protonation of the iminium nitronate. Considering the importance of the pyrrolidine and the acidic function for enamine catalysis, we designed ATCs **1** and **2**, which differ by the C- and N-terminus capping groups. Both compounds were obtained by a slight modification of our previously reported procedure for N-Fmoc protected ATC (see SI).[19] ATC **1** was first evaluated at 10 mol% in model enamine

[a]   J. Aguesseau-Kondrotas, Dr. M. Simon, Dr. B. Legrand, Dr. L. T. Maillard
        Institut des Biomolécules Max Mousseron, UMR CNRS-UM-ENSCM 5247, UFR des Sciences Pharmaceutiques et Biologiques
        15 Avenue Charles Flahault, 34093 Montpellier Cedex 5, France
        E-mail: ludovic.maillard@umontpellier.fr
[b]   Prof. J.-L. Bantigniès
        LC2- UMR 5221 CNRS-UM, Montpellier, France.
[c]   Prof. Y. K. Kang
        Department of Chemistry, Chungbuk National University, Cheongju, Chungbuk 28644, Republic of Korea.
[d]   Dr. D. Dumitrescu
        XRD2 beamline, Elettra - Sincrotrone Trieste S.C.p.A., 34149 Basovizza, Trieste, Italy
[e]   Dr. A. Van der Lee
        Institut Européen des Membranes, UMR CNRS-UM-ENSCM 5635, Montpellier, France
[f]   Prof. J.-M. Campagne, Dr. R. Marcia de Figueiredo
        Institut Charles Gerhardt Montpellier (ICGM), UMR 5253, UMR CNRS-UM-ENSCM Montpellier, France

        Supporting information for this article is given via a link at the end of the document.
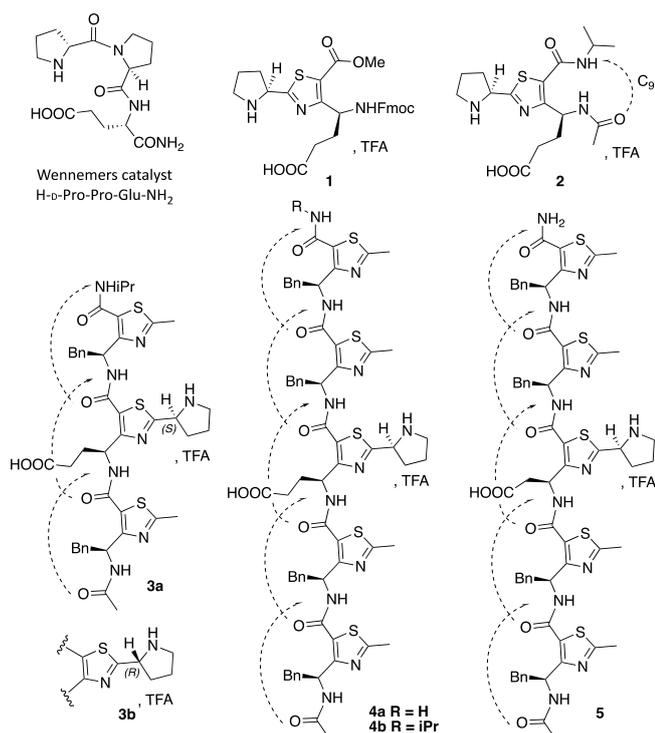
Chart 1. Design of ATC-based enamine catalysts **1** and **2** and introduction of a catalytic centre in heteroaromatic γ-peptides

reactions: 1/ the cross condensation of *p*-nitrobenzaldehyde and acetone; 2-3/ the Michael addition reactions of isovaleraldehyde to dibenzylazodicarboxylate and of cyclohexanone to β-*trans*-nitrostyrene. In the first case, less than 28% *p*-nitrobenzaldehyde was converted after 6h (66% after 7 days), and the reaction led to the Mannich-type product as a major species instead of the desired aldol-type compound (SI). For the addition of isovaleraldehyde to dibenzylazodicarboxylate, the conversion rate was 67% after 2 h (94% after 3.5 days) but no asymmetric induction was observed at 10 mol% catalyst. The effectiveness of ATC **1** was finally established in the nitro-Michael addition reaction of cyclohexanone to β-*trans*-nitrostyrène (Table 1, entries 1-9). The reaction was initially evaluated at 30°C with 10 mol% catalyst as TFA salt and 10 mol% *N*-methylmorpholine as base. **1** showed a high catalytic activity with selectivity toward the *syn* isomer in up to 41% ee for the (*S, R*) enantiomer in isopropanol (Table 1, entry 9). By decreasing the temperature to 4°C, ee increased slightly to 45%. At lower temperature, the conversion decreased to 23 % after four days reaction. Interestingly, using the best experimental conditions, *N*-acetyl-ATC-carboxamide **2** gave higher ee (Table 1, entry 14). This might be explained by a stiffening of the scaffold due to the establishment of an intramolecular C_9-H-bond between the AcCO and *i*PrNH as highlighted by the high deshielding of the NH-*i*Pr amide resonance (δ = 9.64 ppm).[18] Including the catalytic residue in a γ-tripeptide sequence (compound **3a**) enhances the asymmetric induction (*syn/anti* = 99:1; ee = 74%, Table 1, entry 17), suggesting that a folded

three-dimensional structure is likely to contribute to the enantio-selectivity. Esterification of the propanoic chain completely abolishes the catalytic activity confirming its crucial role in the catalysis (data not shown) while inversion of the pyrrolidine chiral centre (compound **3b**) partially inverts the stereoselectivity of the reaction (Table 1, entry 18). In order to explore the influence of the oligomer length, pentapeptides **4a-b** differing by the *C*-term capping were synthesized. As highlighted in Table 1, entries 19-20, **4a-b** conserved a high catalytic selectivity toward the *syn* compound. However, increasing the length to five ATC units marginally improved the ee. Interestingly, shortening the acidic chain (compound **5**) led to a decrease in the β-azodi-carboxylate-nitrostyrene conversion speed, related to a cooperative role of the carboxylic acid function in the catalysis. Finally, we also tried to reduce the charge of catalyst **4a** to 1 mol% but the conversion was very slow (20 % after 2 days). The folding properties of oligomers **4a-b** and **5** at the solution state were then explored by combining circular dichroism, NMR and FT-IR in isopropanol that has been recognized as the best solvent for the catalysis. All compounds shared comparable CD signatures (Figure S25) with a strong positive band centred at

Table 1. Optimization of nitro-Michael addition reaction of cyclohexanone to β-*trans*-nitrostyrene [a]

Entry	Catalyst	Solvent	T (°C)	Yield (%)[b]	syn/anti ratio[c]	ee (%)[d]
1	1	Toluene	30	54	95/5	27
2	1	DMSO	30	82	87/13	29
3	1	CHCl₃	30	81	93/7	27
4	1	THF	30	80	94/6	28
5	1	CH₃CN	30	80	92/8	22
6	1	Hexane	30	88	94/6	31
7	1	MeOH	30	18	95/5	ND
8	1	EtOH	30	98	92/8	34
9	1	*i*PrOH	30	98	96/4	41
10	1	*i*PrOH	4	92	96/4	45
11	2	MeOH	30	44	92/8	ND
12	2	EtOH	30	95	92/8	39
13	2	*i*PrOH	30	94	93/7	50
14	2	*i*PrOH	4	94	93/7	52
15	2	*i*PrOH	-15	16	ND	ND
16	3a	*i*PrOH	30	>99	92/8	64
17	3a	*i*PrOH	4	91	>99/1	74
18	3b	*i*PrOH	4	93	98/2	65ᶠ
19	4a	*i*PrOH	4	>99	>99/1	79
20	4b	*i*PrOH	4	>99	>99/1	77
21	5	*i*PrOH	4	45	>99/1	75

[a] Reaction performed over 16h with 0.1 mmol nitroolefine, 1 mmol cyclohexanone, 0.01 mmol NMM and 0.01 mmol catalyst in 400µl solvent. [b,c] Determined by RP-HPLC at 214 nm. [d] Determined by chiral HPLC (CHIRALPAK IC, *n*-Hexane:*i*-PrOH , vv 8:2, d= 1 ml/min, λ=214 nm). Selectivity toward (2S)-2-[(1R)-2-Nitro-1-phenylethyl]cyclohexanone determined by optical rotation and comparison with reported data in litt.[42] (See Figure S1) [e] Measured after 4 days. . ᶠ (*R, S*) enantiomer was obtained as major compound.

263 nm and a negative maximum at 232 nm. These signatures indicated that all sequences had adopted a similar conformational preference, consistent with the above-described right 9-helix structure for ATC oligomers.[17, 18] The NMR signals were well dispersed and nearly all ^{1}H resonances could be assigned combining COSY, TOCSY and ROESY spectra (Figures S9-10 and S13-14). For both **4a** and **5**, we observed one major conformer and two minor species contributing to 82 %, 16% and 2% for **4a** and 77 %, 12% and 11% for **5**. Interestingly, capping the *C*-term extremity with an isopropyl group (oligomer **4b**) resulted in a single NMR species (Figure S11). The sequential assignments of the major conformers were based on the strong NH(i)/^{γ}CH(i-1) NOE correlations detected on the ROESY spectra. Weak NHi/^{δ}CH(i-1) and ^{γ}CH(i)/^{δ}CH(i+1) sequential NOE connectivities characteristic of the ATC helix were observed along the backbones. Also, we observed strong NH deshielding (> 9 ppm) (Tables S7-S16) as well as ^3J(NH,^{γ}CH) values < 6 Hz (Tables S11-S20) previously recognized as a structural marker related to the formation of the poly-ATC C_9-helix pattern.[18] To gather further experimental evidences on the intramolecular hydrogen bonding, FT-IR experiments were conducted in isopropanol. We especially focused on amide I frequencies (1600-1800 cm^{-1}), which have been formerly recognized as structural markers of the C_9 H-bond network for ATC-containing oligomers.[18, 43] Oligomers **4a-b** and **5** exhibited three absorption components in ν(CO) region (Figure S26). The shoulder contribution at 1705-1710 cm^{-1} is tied to the free acidic lateral chain. Based on the C_9-helix model and on our previously reported studies on ATC oligomers,[18,43] the band at 1674 cm^{-1} should correspond to a combination of the C-terminal carboxamide and of the TFA salt.[44] Finally, the low frequency band at 1630 cm^{-1} was endorsed to the acetyl group at the *N*-terminus of the sequence as well as to the four carbonyls of ATCs 1-4, which are engaged in the H-bond network. After deconvolution of the spectrum into individual Gaussian functions (Table S40), the experimental ratio of free and H-bonded NHs was 3/5 in accordance with the C_9-helix structure. NOEs were finally used as restraints for NMR solution structure calculations using a simulated annealing protocol with AMBER 16.[45] Force field libraries for ATC fragments were generated using the restrained electrostatic potential (RESP) method.[46] Atom charges were derived from the electrostatic potential obtained by DFT calculations with Gaussian 09[47] at the M062X/6-31+G(d) level of theory in vacuum (See SI). The solution structures of **4a** and **5** were solved in implicit solvent using 15 and 16 distance restraints, respectively. As anticipated, they fit to a

tight right-handed 9-helix structure stabilized by C=O(i)$^{...}$HN(i+2) hydrogen bonds (Figure 1 and S23). Importantly, oligomer **5** was successfully crystallized by slow evaporation of an isopropanol solution (CCDC 1894172). ATC oligomer self-assembled into infinite columns linked together by hydrogen bonds between the acid and pyrrolidine side chains (Figures S27-30). It cannot be discounted that such intermolecular association could have occurred in solution, thus explaining the minor species observed in NMR spectra. The ATC γ-peptide **5** adopts the same global helical structure in solution and in a solid state (Figure 1, Table 2). With a distance between pyrrolidine NH and carboxylic acid being 7.1 Å shorter than in the dPPE-NH$_2$ tripeptide,[40] the catalytic centre appeared to be less flexible in ATC-oligomer **4a** than in the Wennemers tripeptide. This lack of adaptability of the catalytic site should explain at least to some extent why the ATC catalysts were less active than their peptidic counterpart.

We then assessed the relationship existing between the placement of the active site along the backbone and the catalytic properties. Four new sequences **6-9** (Figure 2A) were synthesized on solid phase on a Rink-amide ChemMatrix resin following a Fmoc/tBu solid phase peptide synthesis. Each coupling step was performed as previously reported using a mixture of diisopropylcarbodiimide (DIC) and Oxyma Pure® as
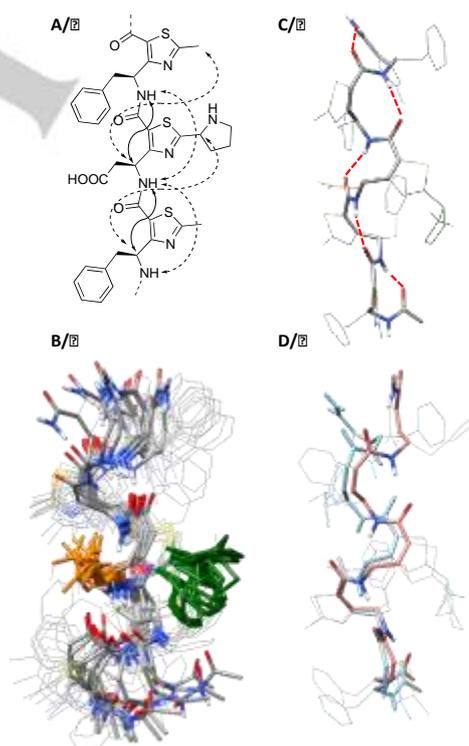
Figure 1. Figure Caption. A/ Characteristic sequential NOE correlations observed for **5**: strong and weak correlations are represented by plain and dotted arrows, respectively. B/ Superimposition of the 20 lowest energy NMR solution structures of **5** in *i*PrOH (Backbone RMSD = 1.421). C/ XRD structure of **5** and D/ superimposition of the XRD (blue) and lowest energy NMR (salmon) structures.

Table 2. Average backbone torsion angles for 9-helical fold γ-peptides **4a**-**b** and **5**.

	ϕ	θ	ζ	ψ
Average NMR values:				
4a	-70 ± 15°	118 ± 8°	-3 ± 2°	-28 ± 13°
4b	-71 ± 17°	119 ± 4°	-4 ± 1°	-35 ± 6°
5	-90 ± 30	116 ± 11	-5 ± 4	-17 ± 7
XRD structure of **5**	-83 ± 11°	117 ± 8°	-1 ± 2°	-36 ± 15°

coupling reagent. After an acidic cleavage from the resin, the peptides were purified by RP-HPLC. With the exception of **6** that precipitated in few minutes in *i*PrOH-d7 thus making NMR characterization impossible, each peptide was submitted to CD, NMR and FT-IR analyses. The observables were comparable for all the oligomers (See SI) suggesting analogous conformational behaviours. The NMR structures of **7-9** were solved and presented in SI (Figure S23 and Table S39). Oligomers **6-9** were then evaluated on the nitro-Michael addition reaction. Three nitro-olefins, i.e. β-*trans*-nitrostyrene, *trans*-4-methyl- and *trans*-4-methoxy-β-nitrostyrene were reacted with cyclohexanone. The data are shown in figure 2B. Whatever the substrate considered, oligomer **4a**, in which the catalytic centre is in the middle of the sequence led to the best percentage of conversion after 16 h reaction (>94%). We observed a slight decrease in the speed

conversion when using the electron rich *trans*-4-methoxy-β-nitrostyrene as reactant. With the exception of the peptide **6**, in which the catalytic ATC was positioned at the *N*-terminus, the asymmetric induction was almost similar for all the peptides (ee = 77-80%) demonstrating that the location of the active site along the backbone had little effect on the stereocontrol. Finally, the steric hindrance around the catalytic centre was increased by introducing an isobutyl group on the thiazole ring of the *N*-terminal residue (Figure 2, oligomer **10**). Despite that the lateral chain pointed on the same face as the acidic function, the global folding has remained unchanged (Figure S23). However, compared to other oligomers, **10** showed a marked preference for the conversion of *trans*-4-methoxy-β-nitrostyrene over the two other olefins. Currently, this result is not totally understood but clearly demonstrates the possibility of modulating the substrate specificity.
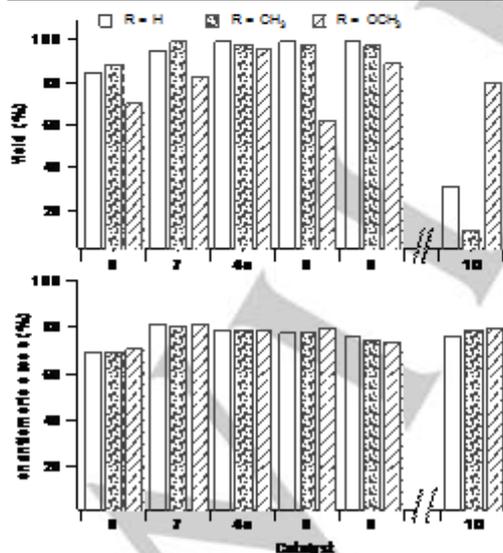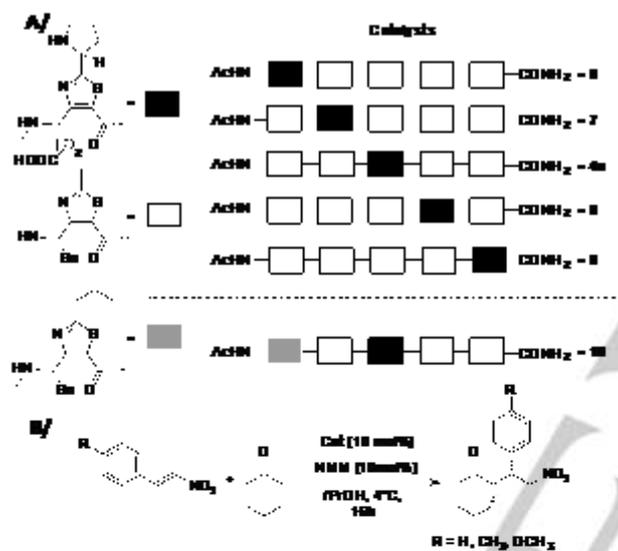
Conclusions

We thus have combined the diverse synthetic toolbox provided by small-molecule catalysis with precise molecular recognition elements made by ATC γ-peptide foldamers. One central feature was to systematically explore the relationship between foldamer size and topology, and the catalytic functions in a model Michael conjugate addition reaction. Through XRD and NMR structural studies, we demonstrated the potential of the ATC scaffold as a versatile platform for the *de novo* design of modular catalysts. Design of a true substrate-binding pocket represents the next challenge for the conception of an enzyme-like catalyst.

Experimental Section

Commercially available reagents and solvents were used without any further purification. Reactions were monitored by HPLC using an analytical Chromolith® Speed Rod RP-C18 185 Pm column (50 x 4.6 mm, 5 μm) using a flow rate of 5.0 ml/min, and gradients from 100/0 to 0/100 eluents A/B over 3 (condition A) or 5 min (condition B), in which eluents A = H2O / TFA 0.1% and B = CH3CN / TFA 0.1%. Detection was done at 214 nm and 254 nm using a Photodiode Array Detector. Retention times are reported as follows: LC: rt = (min). 1H and 13C NMR spectra were recorded at room temperature in deuterated solvents. Chemical shifts (δ) are given in parts per million relative to TMS or relative to the solvent [1H: δ (CDCl3) = 7.24 ppm; 13C: δ (CDCl3) = 77.2 ppm]. The following abbreviations are used to designate the signal multiplicities: s (singlet), d (doublet), dd (doublet doublet), t (triplet), q (quartet), m (multiplet), br (broad). Analytical Thin-Layer Chromatography (TLC) was performed using aluminium-backed silica gel plates coated with a 0.2 mm thickness of silica gel or with aluminium oxide 60 F254, neutral. LC-MS spectra (ESI) were recorded on an HPLC using an analytical Chromolith Speed Rod RP-C18 185 Pm column (50 x 4.6 mm, 5 μm) using a flow rate of 3.0 mL/min, and gradients of 100/0 to 0/100 eluents A/B over 2.5 min, in which eluents solvent A = H2O / HCOOH 0.1% and solvent B = CH3CN /HCOOH 0.1%. High-Resolution Mass Spectrometric analyses were performed with a time-of-flight (TOF) mass spectrometer fitted with an Electrospray Ionization Source (ESI). All measurements were performed in the positive ion mode. Melting points (mp) are uncorrected and were recorded on a capillary melting point apparatus. Enantiomeric excesses were determined by Chiral HPLC analysis using a Chiralpak® IC column

Figure 2. A/ Sequences of peptides **6-9**. B/ Evaluation of the Nitro-Michael addition reaction using β-*trans*-nitrostyrène (R = H), *trans*-4-methyl- (R = CH₃) and *trans*-4-methoxy-β-nitrostyrene (R = OCH₃) and oligomers **4a** and **6-9** as catalysts.

(250 x 4.6 mm) with n-hexane/isopropanol (80/20) as eluent or Chiralpak® IA column (250 x 4.6 mm) with n-hexane/isopropanol (90/10) as eluent and a flow rate of 1 ml/min. Fmoc-ATC-OH were prepared according to reported procedures[19] Syntheses of compounds **1**, **2**, **4b** are described in SI.

General procedure for peptide solid phase synthesis: Solid-phase synthesis of oligomers **3**, **4a**, **5-10** was performed on a ChemMatrix® Rink Amide resin loaded at 0.49 mmol/g using Fmoc/*t*-Bu chemistry. Resin was soaked in *N*-methylpyrrolidone (NMP) for 5-10 minutes and filtered. Fmoc-ATC-OH (2.0 equiv.), DIC (2.0 equiv.), Oxyma Pure (2.0 equiv.) and NMP were added in this order for each peptide coupling (overnight at r.t.). Resin was washed using the following procedure: 3 × DMF, 3 × DCM, 1 × DMF, 1 × DCM. Each coupling was followed by a capping step with Ac$_2$O/DCM 1/1 vv solution (1 × 5 min at r.t.) and washed. Deprotection at the *N*-terminus was performed using a 20% piperidine/DMF solution (3 × 10 min at r.t.) and the resin was then washed before the next coupling. Deprotection and coupling steps were monitored by Kaiser test.

Nitro-Michael addition reactions: The catalyst (0.0037 mmol, 0.1 equiv.) was dissolved in 150μL of a solution of NMM/iPrOH (11 μL in 4mL). The nitrostyrene (0.037 mmol, 1.0 equiv.) and the cyclohexanone (38.5 μL, 0.37 mmol, 10.0 equiv.) were then added and the reaction mixture was stirred at 4°C for 16 hours. Monitoring was done by diluting 5μL of the reaction mixture in 400μL MeOH. 5 μL of this solution were injected for the HPLC analysis performed with Chromolith Speed Rod RP-C18 185 Pm column (50 x 4.6 mm, 5 μm) using a flow rate of 3.0 mL/min, and gradients of 100/0 to 0/100 eluents A/B over 3 min, in which eluents solvent A = H$_2$O / TFA 0.1% and solvent B = CH$_3$CN / TFA 0.1%. Enantiomeric excesses were determined by Chiral HPLC analysis using method A: a Chiralpak® IC column (250 x 4.6 mm) with *n*-hexane/isopropanol (80/20) as eluent at a flow rate of 1 ml/min or method B: a Chiralpak® IA column (250 x 4.6 mm) with *n*-hexane/isopropanol (90/10) as eluent at a flow rate of 1 ml/min. See Supporting Information for HPLC profiles.

NMR experiments: All spectra were recorded on a Bruker Avance 600 AVANCE III spectrometer equipped with a 5 mm triple-resonance cryoprobe (^{1}H, ^{13}C, ^{15}N). Homonuclear 2-D spectra DQF-COSY, TOCSY (DIPSI2) and ROESY were typically recorded in the phase-sensitive mode using the States-TPPI method as data matrices of 256-512 real (t$_1$) × 2048 (t$_2$) complex data points; 8-48 scans per t$_1$ increment with 1.0 s recovery delay and spectral width of 6009 Hz in both dimensions were used. The mixing times were 60 ms for TOCSY and 350-450 ms for the ROESY and the NOESY experiments. In addition, 2D heteronuclear spectra ^{15}N, ^{13}C-HSQC and ^{13}C-HSQC-TOCSY were acquired to fully assign the oligomers (8-32 scans, 256-512 real (t$_1$) × 2048 (t$_2$) complex data points). Spectra were processed with Topspin (Bruker Biospin) and visualized with Topspin or NMRview on a Linux station. The matrices were zero-filled to 1024 (t$_1$) x 2048 (t$_2$) points after apodization by shifted sine-square multiplication and linear prediction in the F1 domain. Chemical shifts were referenced to the solvent.

Molecular modelling studies: Force field libraries for ATC fragments were generated using the restrained electrostatic potential (RESP) method. Atom charges were derived from the electrostatic potential obtained by DFT calculations with Gaussian 09[47] at the M062X/6-31+G(d) level of theory in vacuum. The computed electrostatic potential (ESP) was fit using RESP charge fitting in antechamber. Structure calculations. ^{1}H chemical shifts were assigned according to classical procedures. NOE cross-peaks were integrated and assigned within the NMRView software[48]. The volume of a ROE between methylene pair protons or ortho phenyl protons was used as a reference of 1.8 Å or 2.48 Å

respectively. The lower bound for all restraints was fixed at 1.8 Å and upper bounds at 2.7, 3.3 and 5.0 Å, for strong, medium and weak correlations, respectively. Pseudo-atoms corrections of the upper bounds were applied for unresolved aromatic, methylene and methyl protons signals as described previously[49]. Structure calculations were performed with AMBER 16[45] in three stages: cooking, simulated annealing in vacuum and refinement in a solvent box. The cooking stage was performed at 600 K to generate 100 initial random structures. SA calculations were carried during 20 ps (20000 steps, 1 fs long) as described elsewhere. First, the temperature was risen quickly and was maintained at 600 K for the first 5000 steps, then the system was cooled gradually from 600 K to 100 K from step 5001 to 18000 and finally the temperature was brought to 0 K during the 2000 remaining steps. For the 3000 first steps, the force constant of the distance restraints was increased gradually from 2.0 kcal.mol^{-1}.Å to 20 kcal.mol^{-1}.Å. For the rest of the simulation (step 3001 to 20000), the force constant is kept at 20 kcal.mol^{-1}.Å. The calculations were launched using the generalized born solvation model. The 20 lowest energy structures with no violations > 0.3 Å were considered as representative of the peptide structure. The representation and quantitative analysis were carried out using Ptraj, MOLMOL[50] and PyMOL (Delano Scientific).

Acknowledgements

[1]   A. Illanes, *Enzyme Biocatalysis Principles and Applications*, Springer Science & Business Media, **2008**.

[2]   O. Kirk, T. V. Borchert and C. C. Fuglsang, *Curr. Opin. Biotechnol.*, **2002**, *13*, 345-351.

[3]   G. D. Haki and S. K. Rakshit, *Bioresour. Technol.*, **2003**, *89*, 17-34.

[4]   S. J. Miller, *Acc. Chem. Res.*, **2004**, *37*, 601-610.

[5]   E. R. Jarvo and S. Miller, *Tetrahedron*, **2002**, *58*, 2481-2495.

[6]   H. Wennemers, *Chem. Commun.*, **2011**, *47*, 12036-12041.

[7]   E. A. Davie, S. M. Mennen, Y. Xu and S. J. Miller, *Chem. Rev.*, **2007**, *107*, 5759-5812.

[8]   P. E. Coffey, K. H. Drauz, S. M. Roberts, J. Skidmore and J. A. Smith, *Chem. Commun.*, **2001**, 2330-2331.

[9]   T. Hasegawa, Y. Furusho, H. Katagiri and E. Yashima, *Angew. Chem. Int. Ed. Engl.*, **2007**, *46*, 5885-5888.

[10]   G. Maayan, M. D. Ward and K. Kirshenbaum, *Proc. Natl. Acad. Sci. USA*, **2009**, *106*, 13679-13684.

[11]   M. M. Muller, M. A. Windsor, W. C. Pomerantz, S. H. Gellman and D. Hilvert, *Angew. Chem. Int. Ed. Engl.*, **2009**, *48*, 922-925.

[12]   P. S. Wang, J. B. Nguyen and A. Schepartz, *J. Am. Chem. Soc.*, **2014**, *136*, 6810-6813.

[13]   B. A. Le Bailly, L. Byrne and J. Clayden, *Angew. Chem. Int. Ed. Engl.*, **2016**, *55*, 2132-2136.

[14]   D. Becart, V. Diemer, A. Salaun, M. Oiarbide, Y. R. Nelli, B. Kauffmann, L. Fischer, C. Palomo and G. Guichard, *J. Am. Chem. Soc.*, **2017**, *139*, 12524-12532.

[15]   Z. C. Girvin and S. H. Gellman, *J. Am. Chem. Soc.*, **2018**, *140*, 12476-12483.

[16]   C. M. Goodman, S. Choi, S. Shandler and W. F. DeGrado, *Nat. Chem. Biol.*, **2007**, *3*, 252-262.

FULL PAPER

[17] L. Mathieu, B. Legrand, C. Deng, L. Vezenkov, E. Wenger, C. Didierjean, M. Amblard, M. C. Averlant-Petit, N. Masurier, V. Lisowski, J. Martinez and L. T. Maillard, *Angew. Chem. Int. Ed. Engl.*, **2013**, *52*, 6006-6010.

[18] C. Bonnel, B. Legrand, J. L. Bantignies, H. Petitjean, J. Martinez, N. Masurier and L. T. Maillard, *Org. Biomol. Chem.*, **2016**, *14*, 8664-8669.

[19] L. Mathieu, C. Bonnel, N. Masurier, L. T. Maillard, J. Martinez and V. Lisowski, *Eur. J. Org. Chem.*, **2015**, 2262-2270.

[20] M. Simon, L. M. A. Ali, K. E. Cheikh, J. Aguesseau, M. Gary-Bobo, M. Garcia, A. Morère and L. T. Maillard, *Chem. Eur. J.*, **2018**, *24*, 11426-11432.

[21] S. Mukherjee, J. W. Yang, S. Hoffmann and B. List, *Chem. Rev.*, **2007**, *107*, 5471-5569.

[22] Pihko P.M., Majander I., Erkkilä A. in *Enamine Catalysis. In: List B. (eds) Asymmetric Organocatalysis. Topics in Current Chemistry, vol 291.* Springer, Berlin, Heidelberg. **2010**

[23] F. Giacalone, M. Gruttadauria, P. Agrigento and R. Noto, *Chem. Soc. Rev.*, **2012**, *41*, 2406-2447.

[24] W. Notz, F. Tanaka and C. F. Barbas, 3rd, *Acc. Chem. Res.*, **2004**, *37*, 580-591.

[25] B. List, *J. Am. Chem. Soc.*, **2000**, *112*, 9336-9337.

[26] B. List, P. Pojarliev, W. T. Biller and H. J. Martin, *J. Am. Chem. Soc.*, **2002**, *124*, 827-833.

[27] Y. Hayashi, W. Tsuboi, I. Ashimine, T. Urushima, M. Shoji and K. Sakai, *Angew. Chem. Int. Ed. Engl.*, **2003**, *42*, 3677-3680.

[28] F. Tanaka and C. F. Barbas, in *Enantioselective Organocatalysis: Reactions and experimental procedures (Ed.: P.I. Dalko), Wiley-VCH, Weinheim*, **2007**, p.19.

[29] S. P. Brown, M. P. Brochu, C. J. Sinz and D. W. MacMillan, *J. Am. Chem. Soc.*, **2003**, *125*, 10808-10809.

[30] Z. G., *Angew. Chem. Int. Ed. Engl.*, **2003**, *42*, 4247-4250.

[31] Y. Hayashi, J. Yamaguchi, T. Sumiya and M. Shoji, *Angew. Chem. Int. Ed. Engl.*, **2004**, *43*, 1112-1115.

[32] A. Bogevig, H. Sunden and A. Cordova, *Angew. Chem. Int. Ed. Engl.*, **2004**, *43*, 1109-1112.

[33] B. List, *J. Am. Chem. Soc.*, **2002**, *124*.

[34] N. Kumaragurubaran, K. Juhl, W. Zhuang, A. Bogevig and K. A. Jorgensen, *J. Am. Chem. Soc.*, **2002**, *124*, 6254-6255.

[35] A. Bogevig, K. Juhl, N. Kumaragurubaran, W. Zhuang and K. A. Jorgensen, *Angew. Chem. Int. Ed. Engl.*, **2002**, *41*, 1790-1793.

[36] M. Wiesner, J. D. Revell, S. Tonazzi and H. Wennemers, *J. Am. Chem. Soc.*, **2008**, *130*, 5610-5611.

[37] M. Wiesner, J. D. Revell and H. Wennemers, *Angew. Chem. Int. Ed. Engl.*, **2008**, *47*, 1871-1874.

[38] M. Wiesner, M. Neuburger and H. Wennemers, *Chem. Eur. J.*, **2009**, *15*, 10103-10109.

[39] M. Wiesner, G. Upert, G. Angelici and H. Wennemers, *J. Am. Chem. Soc.*, **2010**, *132*, 6-7.

[40] T. Schnitzer and H. Wennemers, *J. Am. Chem. Soc.*, **2017**, *139*, 15356-15362.

[41] J. Duschmale, J. Wiest, M. Wiesner and H. Wennemers, *Chem. Sci.*, **2013**, *4*, 1312-1318.

[42] Y. Xu and A. Cordova, *Chem. Commun.*, 2006, 460-462.

[43] C. Bonnel, B. Legrand, M. Simon, J. Martinez, J. L. Bantignies, Y. K. Kang, E. Wenger, F. Hoh, N. Masurier and L. T. Maillard, *Chem. Eur. J.*, **2017**, *23*, 17584-17591.

[44] S. Roux, E. Zékri, B. Rousseau, M. Paternostre, J. C. Cintrat and N. Fay, *J. Pept. Sci.*, **2008**, *14*, 354-359.

[45] D.A. Case, R.M. Betz, D.S. Cerutti, T.E. Cheatham, III, T.A. Darden, R.E. Duke, T.J. Giese, H. Gohlke, A.W. Goetz, N. Homeyer, S. Izadi, P. Janowski, J. Kaus, A. Kovalenko, T.S. Lee, S. LeGrand, P. Li, C. Lin, T. Luchko, R. Luo, B. Madej, D. Mermelstein, K.M. Merz, G. Monard, H. Nguyen, H.T. Nguyen, I. Omelyan, A. Onufriev, D.R. Roe, A. Roitberg, C. Sagui, C.L. Simmerling, W.M. Botello-Smith, J. Swails, R.C. Walker, J. Wang, R.M. Wolf, X. Wu, L. Xiao and P.A. Kollman, AMBER 2016, University of California, San Francisco, **2016**

[46] J. Wang, P. Cieplak and P. Kollman, *J. Comput. Chem.*, **2000**, *12*, 1049-1074.

[47] M. J. T. Frisch, G. W.; Schlegel, H. B.; Scuseria, G. E.; Robb, M. A.; Cheeseman, J. R.; Scalmani, G.; Barone, V.; Mennucci, B.; Petersson, G. A.; Nakatsuji, H.; Caricato, M.; Li, X.; Hratchian, H. P.; Izmaylov, A. F.; Bloino, J.; Zheng, G.; Sonnenberg, J. L.; Hada, M.; Ehara, M.; Toyota, K.; Fukuda, R.; Hasegawa, J.; Ishida, M.; Nakajima, T.; Honda, Y.; Kitao, O.; Nakai, H.; Vreven, T.; Montgomery, J. A., Jr.; Peralta, J. E.; Ogliaro, F.; Bearpark, M.; Heyd, J. J.; Brothers, E.; Kudin, K. N.; Staroverov, V. N.; Kobayashi, R.; Normand, J.; Raghavachari, K.; Rendell, A.; Burant, J. C.; Iyengar, S. S.; Tomasi, J.; Cossi, M.; Rega, N.; Millam, J. M.; Klene, M.; Knox, J. E.; Cross, J. B.; Bakken, V.; Adamo, C.; Jaramillo, J.; Gomperts, R.; Stratmann, R. E.; Yazyev, O.; Austin, A. J.; Cammi, R.; Pomelli, C.; Ochterski, J. W.; Martin, R. L.; Morokuma, K.; Zakrzewski, V. G.; Voth, G. A.; Salvador, P.; Dannenberg, J. J.; Dapprich, S.; Daniels, A. D.; Farkas, O.; Foresman, J. B.; Ortiz, J. V.; Cioslowski, J.; Fox, D. J., in Gaussian 09, Revision D.01; Gaussian, Inc.: Wallingford, CT, **2013**.

[48] B. A. Johnson, R. A. Blevins, *J. Biomol. NMR* **1994**, *4*, 603

[49] Wüthrich, K. in *NMR of Proteins and Nucleic acids*, Wiley-Interscience: New York, **1986**

[50] R. Koradi, M. Billeter, K. Wuthrich, *J. Mol. Graph.* **1996**, *14*, 51

Entry for the Table of Contents (Please choose one layout)

Layout 2:

FULL PAPER

Julie Aguesseau-Kondrotas, Matthieu Simon, Baptiste Legrand, Jean-Louis Bantigniès, Young Kee Kang, Dan Dumitrescu, Arie Van der Lee, Jean-Marc Campagne, Renata Marcia de Figueiredo[*] and Ludovic T. Maillard[*][a]
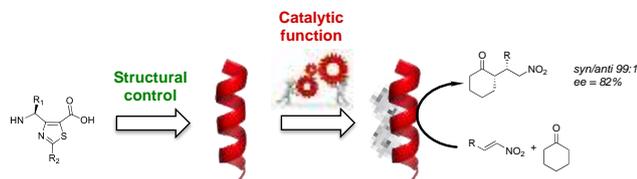
tWe herein explored the ability of heterocyclic γ–peptide scaffolds for enamine catalysis. One central feature was to determine how the catalytic activity and the transfer of chiral information might be under the control of the conformational behaviours of the oligomer.